Kinetics of Two-Dimensional Phase Transitions of Sulfide and Halide Ions on Ag(111)

Massimo Innocenti, Maria Luisa Foresti, Antonio Fernandez,† Francesca Forni, and Rolando Guidelli*

Chemistry Department, University of Florence, Via G. Capponi, 9, 50121-Florence, Italy

Received: June 1, 1998; In Final Form: September 18, 1998

The kinetics of two-dimensional phase transitions of sulfide, iodide, bromide, and chloride ions on Ag(111) was investigated at anionic concentrations ranging from 1×10^{-4} to 1×10^{-3} M by measuring the time dependence of the charge following steps from a potential negative enough to exclude anionic adsorption to a potential in the range of stability of either the first or the second, more compressed, ordered overlayer of the anions. The kinetic behavior is interpreted by a model that accounts for diffusion-controlled random adsorption of the anions, followed by progressive polynucleation and growth. When stepping to the potential range of stability of the second overlayer, the kinetic behavior is accounted for by assuming that the passage from total desorption to the second overlayer occurs via the intermediate formation of the first one.

Introduction

The kinetic and structural features of two-dimensional (2D) phase transitions on single-crystal faces have received increasing attention in recent years. A large amount of work has been devoted to 2D phase transitions of organic compounds (mainly pyrimidine and purine bases) on Au(111)[1−7] and Ag(111)[8−11] and to those accompanying the underpotential deposition of metals on Au, Ag, and Pt single-crystal faces.[12−25] In many cases, structural evidence for the formation of 2D long-range ordered overlayers was obtained from in situ scanning tunneling microscopy (STM) images with atomic or molecular resolution. On the other hand, kinetic evidence was obtained from potentiostatic current vs time curves showing partial control by polynucleation and growth (PG). These current transients are normally characterized by an exponential decay, which precedes the typical rising section, followed by the gradual decay toward zero current, encountered in PG processes on mercury. The particular shape of current transients has been usually explained by postulating two parallel pathways. According to Kolb et al.,[5,26] the initial exponential decay is due to random adsorption (RA) at microscopic surface inhomogeneities that do not allow the formation of a 2D laterally organized condensed film; the subsequent current maximum is ascribed to PG on the structurally well-ordered portion of the electrode surface. A somewhat different explanation for the shape of current transients was provided by Bhattacharjee and Rangarajan.[27] According to these authors, RA and PG proceed in parallel on the same electrode surface, regarded as homogeneous. Only a weak interference between the two processes is postulated. Thus, the surface area covered by the condensed film is assumed not to be available for RA; analogously, the surface area covered by randomly adsorbed molecules is assumed not to be available for PG. While the former assumption is quite reasonable, the latter is less obvious, since it excludes the progressive incorporation of randomly adsorbed molecules into growing clusters of the condensed phase. Account of such an incorporation was taken by de Levie et al.[28,29] A similar approach was taken in this laboratory in treating the 2D phase transitions of uracil on Ag(111).[10]

In the past years, structural evidence for the formation of ordered halide overlayers on Ag,[30,31] Au,[32−42] and Pt[43−46] single-crystal electrodes has been provided by using in situ scanning probe and X-ray techniques. Despite this, investigations on the kinetics of formation of these overlayers are lacking, with the only exception of a kinetic study of 2D phase transition of bromide ion on Au(111).[47] The same is true for other inorganic anions giving rise to overlayers on single-crystal faces of noble metals, except for a kinetic study of sulfate 2D condensation on stepped Au(111).[48]

The present paper deals with a kinetic investigation of the 2D phase formation of sulfide, iodide, bromide, and chloride overlayers on Ag(111). It will be shown that, under properly selected experimental conditions, the condensed phases are formed by diffusion-controlled RA of the chemisorbed anions, followed by their progressive nucleation and by growth of the resulting clusters. This mechanism is therefore quite general and is likely to be followed by other inorganic ions giving rise to 2D phase transitions on single-crystal faces. The kinetic treatment of this mechanism accounts satisfactorily for the experimental behavior.

Experimental Section

Merck Suprapur KI, KBr, and KCl were baked at 400 °C to remove organic impurities. Merck Suprapur NaOH and Aldrich analytical reagent grade Na_2S were used without further purification. Jansen analytical reagent grade KPF_6 was purified as described in refs 49 and 50. The water used was obtained from light mineral water by distilling it once and by then distilling the water so obtained from alkaline permanganate while discarding the heads. Sulfide solutions were freshly prepared just before the beginning of each series of measurements. The working electrodes were cylindrical silver crystals grown in a graphite crucible, oriented by X-rays and cut according to the Bridgman technique.[51] These electrodes were polished with successively finer grades of alumina power down to 0.3 μm (Buehler Micropolish II) and then annealed in a muffle

† On leave from University of Cordoba (Spain).

10.1021/jp982427m CCC: $15.00
Published on Web 11/10/1998

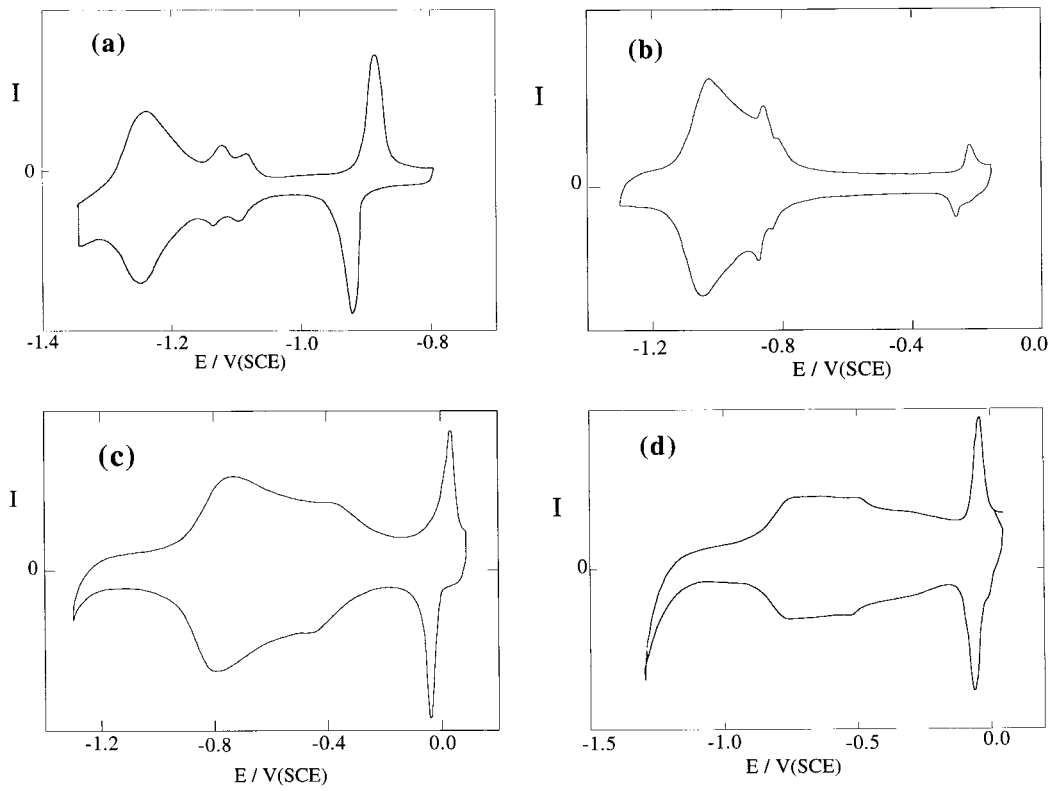

Figure 1. Cyclic voltammograms on Ag(111) from solutions of 5×10^{-4} M Na_2S + 0.15 M NaOH (a), 5×10^{-4} M KI + 0.15 M NaOH (b), 5×10^{-4} M KBr + 0.05 M KPF_6 (c), and 5×10^{-4} M KCl + 0.05 M KPF_6 (d).

furnace under vacuum for 30 min at 650 °C. Before each electrochemical measurement the electrode was polished chemically with CrO_3 according to the procedure described in ref 52. After polishing, the electrode surface was soaked in concentrated sulfuric acid for about 20 min and then rinsed thoroughly with water.

A gold wire was used as a counter electrode, and an external saturated calomel electrode (SCE) served as reference; all potentials are referred to this electrode. The four-electrode potentiostatic system by Herrmann et al.[53] was employed to minimize the noise, and positive feedback circuitry was utilized to correct for the uncompensated resistance. The hanging solution method[54] was employed. The cell was water-jacketed and thermostated at 25 ± 0.2 °C. The solution was deaerated with argon, which was bubbled into the solution before measurements and flown over the solution during them. The cylindrical single-crystal electrode was held by a silver wire sealed into a glass tube which was secured to a movable stand. Cyclic voltammetric and chronocoulometric measurements were carried out under the control of a Data General DG10 microcomputer: the voltage signal, modulated according to the technique employed, was generated by the microcomputer through digital-to-analog conversion and applied to the cell via an Amel model 551 fast-rise potentiostat. In the cyclic voltammetric measurements the potential was scanned between two chosen values, and the current response from the cell was recorded by a 7090A HP plotting system. The wholly computerized experimental apparatus permitted us to switch from one technique to another, via software, while keeping the working electrode under a controlled applied potential.

Results

Figure 1 shows the cyclic voltammograms of sulfide, iodide, bromide, and chloride ions on Ag(111). Proceeding toward more positive potentials, all voltammetric curves show one or more rounded humps followed by a relatively flat region and by a sharp peak. With the only exception of chloride, in the flat region scanning tunneling microscopy reveals the presence of an ordered $(\sqrt{3} \times \sqrt{3})R30°$ structure.[31,55,56] The subsequent sharp peak marks a first-order phase transition from the $(\sqrt{3} \times \sqrt{3})R30°$ structure to a more compressed ordered structure. In the case of sulfide ions, this is a $(\sqrt{7} \times \sqrt{7})R19.1°$ structure in which each lattice site is occupied by a trimer of sulfide ions.[55] Bromide ions also show a $(\sqrt{7} \times \sqrt{7})R19.1°$ structure, which differs from that shown by sulfide ions in that, along any given row, the ions are adsorbed in a succession of two hollow sites and one top site.[31] In view of their large size, iodide ions cannot form a $(\sqrt{7} \times \sqrt{7})R19°$ structure, but rather give rise to a slightly less compressed structure, namely a $(8 \times 8)R0°$ structure, in which the iodide ions at the vertexes of each elementary cell occupy top sites and constitute the tops of corrugations with hexagonal symmetry in the STM image.[31] Slightly different conclusions were drawn by Ocko et al.[56] using surface X-ray scattering. According to these authors, a progressive positive shift of the applied potential causes the iodide overlayer on Ag(111) to pass from a $(\sqrt{3} \times \sqrt{3})R30°$ structure to a uniaxial-incommensurate $c(p \times \sqrt{3})$ structure and then to a rotated-hexagonal phase. The latter phase, with a nearest-neighbor iodide spacing of 4.59 Å, is similar to our (8×8) structure, with a spacing of 4.45 Å. Chloride adsorption gives rise to an ordered $(1.38 \times 1.38)R0°$ structure[30,57] only at potentials positive to the sharp peak in the voltammogram of Figure 1, curve d, which marks a disorder−order 2D phase transition.

2D phase transitions on solid electrodes are normally faster than on mercury, quite probably due to the numerous surface defects that act as preferential sites for nucleation, i.e., nucleation centers. To single out the kinetics of PG of the anions under

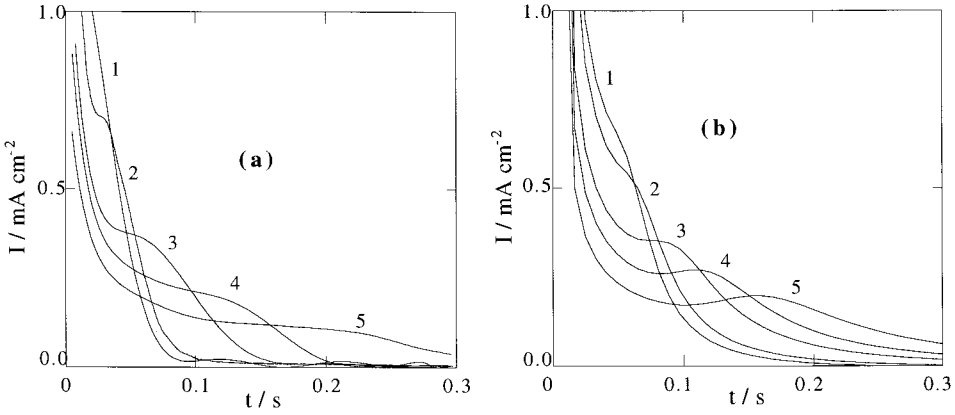

Figure 2. (a) Current vs time curves obtained on Ag(111) from 0.15 M NaOH solutions containing 8.55×10^{-4} (1), 7.48×10^{-4} (2), 5.35×10^{-4} (3), 4.28×10^{-4} (4), and 3.20×10^{-4} M (5) KI by stepping from −1.50 to −0.50 V. (b) Corresponding current vs time curves calculated as described in the text.

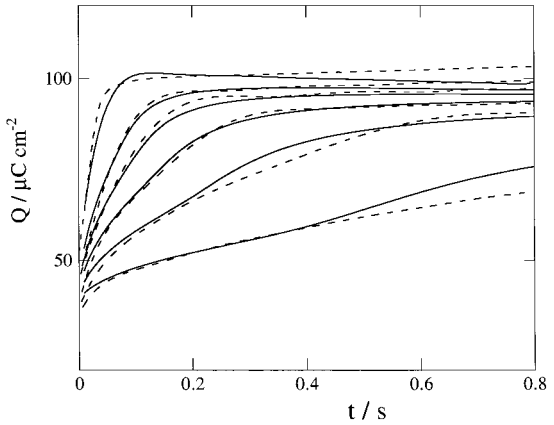

Figure 3. Charge vs time curves for iodide adsorption on Ag(111) obtained from 0.15 M NaOH solutions by stepping from −1.50 to −0.50 V. Proceeding from left to right, the KI concentrations are 8.55×10^{-4}, 5.35×10^{-4}, 4.28×10^{-4}, 3.20×10^{-4}, 2.14×10^{-4}, and 1.07×10^{-4} M. The dashed curves are experimental plots; the solid ones were calculated as described in the text.

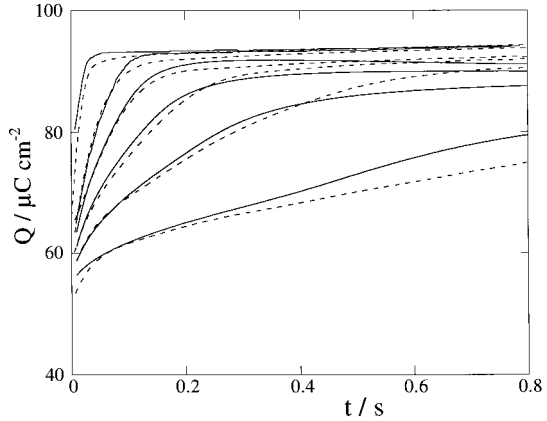

Figure 4. Charge vs time curves for bromide adsorption on Ag(111) obtained from 0.05 M KPF_6 solutions by stepping from −1.50 to −0.35 V. Proceeding from left to right, the KBr concentrations are 8.91×10^{-4}, 5.58×10^{-4}, 4.47×10^{-4}, 3.35×10^{-4}, 2.24×10^{-4}, and 1.12×10^{-4} M. The dashed curves are experimental plots; the solid ones were calculated as described in the text.

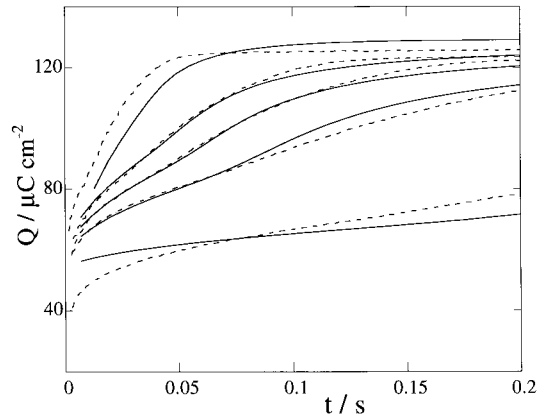

Figure 5. Charge vs time curves for chloride adsorption on Ag(111) obtained from 0.05 M KPF_6 solutions by stepping from −1.50 to +0.15 V. Proceeding from left to right, the KCl concentrations are 7.67×10^{-4}, 4.79×10^{-4}, 3.83×10^{-4}, 2.87×10^{-4}, and 1.91×10^{-4} M. The dashed curves are experimental plots; the solid ones were calculated as described in the text.

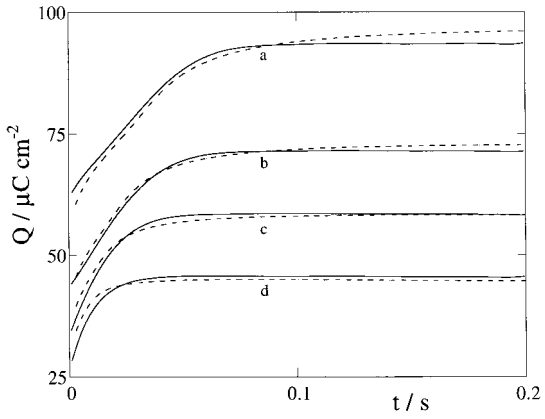

Figure 6. Charge vs time curves on Ag(111) obtained from a solution of 6×10^{-4} M KI + 0.15 M NaOH by stepping from −1.50 (a), −1.10 (b), −1.05 (c), and −1.00 V (d) to the same final potential −0.50 V. The experimental surface coverage θ by iodide ion equals 0 at −1.50 V (a), 0.18 at −1.10 V (b), 0.36 at −1.05 V (c), and 0.54 at −1.00 V (d) The dashed curves are experimental plots; the solid ones were calculated as described in the text.

study, it was therefore necessary to step from an initial potential negative enough to exclude their adsorption to a final potential where 2D condensation takes place. It was also necessary to adopt solutions dilute enough (from 10^{-4} to 10^{-3} M) to cause adsorption to occur under partial diffusion control over a time period much longer than that required for double-layer charging. Under these conditions, the initial RA drives a process of PG whose kinetics becomes slow enough to be followed. Figure 2a shows curves of the current I vs time t for iodide, as obtained by stepping from a potential negative enough to exclude iodide

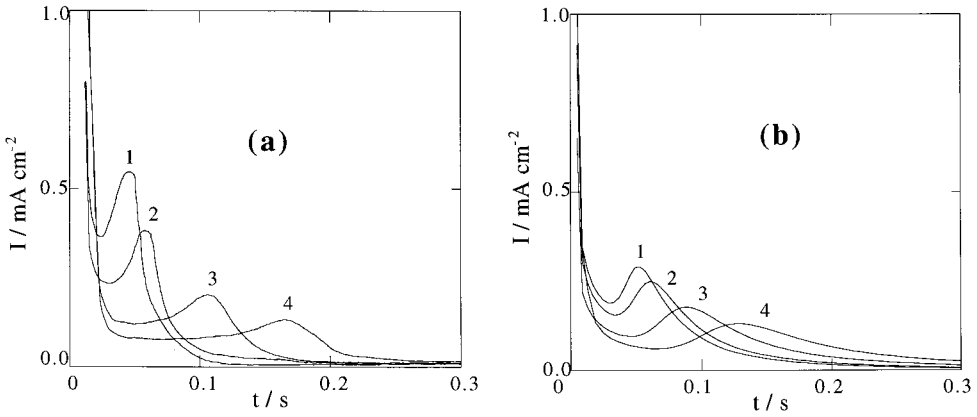

Figure 7. (a) Current vs time curves obtained on Ag(111) from 0.05 M KPF_6 solutions containing 8.91×10^{-4} (1), 7.80×10^{-4} (2), 5.58×10^{-4} (3), and 4.47×10^{-4} (4) KBr by stepping from −1.50 to −0.05 V. (b) Corresponding current vs time curves calculated as described in the text.

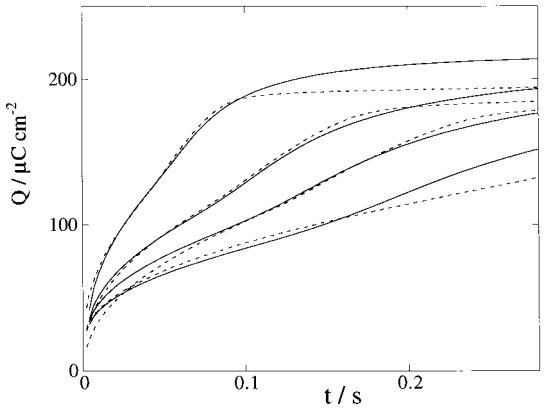

Figure 8. Charge vs time curves for sulfide adsorption on Ag(111) obtained from 0.15 M NaOH solutions by stepping from −1.35 to −0.80 V. Proceeding from left to right, the Na_2S concentrations are 7.80×10^{-4}, 4.87×10^{-4}, 4.38×10^{-4}, and 2.92×10^{-4} M. The dashed curves are experimental plots; the solid ones were calculated as described in the text.

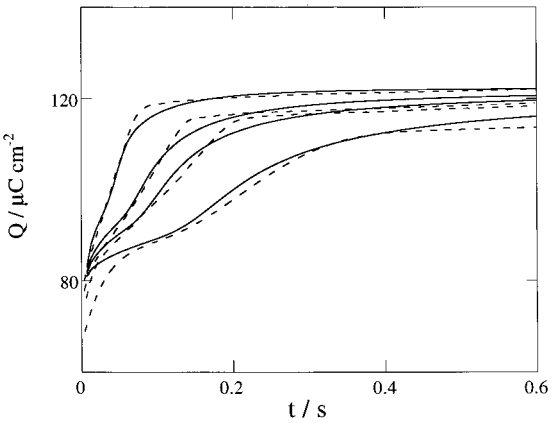

Figure 9. Charge vs time curves for iodide adsorption on Ag(111) obtained from 0.15 M NaOH solutions by stepping from −1.50 to −0.20 V. Proceeding from left to right, the KI concentrations are 7.48 $\times 10^{-4}$, 5.35×10^{-4}, 4.28×10^{-4}, and 3.20×10^{-4} M. The dashed curves are experimental plots; the solid ones were calculated as described in the text.

adsorption to a potential in the range of stability of the $(\sqrt{3} \times \sqrt{3})R30°$ structure. These curves exemplify the behavior of iodide, bromide, and chloride adsorption as we step into the range of stability of the first condensed phase (i.e., the $(\sqrt{3} \times \sqrt{3})R30°$ overlayer for iodide and bromide and the $(1.38 \times 1.38)R0°$ overlayer for chloride). The curves in Figure 2a, relative to different concentrations of iodide, do not show the exponential decay typical of rate control by diffusion, RA, or both. Rather, they exhibit a shoulder that is longer the lower the anion concentration. As expected, the corresponding curves of the charge $Q(t)$ vs time t in Figures 3−5 show an approximately linear section in the same time interval over which the I vs t curves show the shoulder. As the initial potential E_i is gradually shifted toward more positive values while keeping the final potential E constant, the charge transients undergo a gradual change in shape that is exemplified in Figure 6 for the case of iodide adsorption. As long as E_i remains in the potential range over which iodide adsorption is entirely negligible, the charge transients shift downward without changing their shape: the vertical shift is just equal to the difference in the charge density $\sigma_M(E_i)$ on the metal between the different E_i values. However, as soon as the initial potential starts to be characterized by an appreciable surface coverage θ by randomly adsorbed anions, the charge transient attains its constant limiting value at progressively shorter times.

A different behavior is exhibited by the I vs t curves for sulfide, iodide, and bromide adsorption, as obtained by stepping from a potential of total desorption to a potential in the range of stability of the second, more compressed overlayer (i.e., the $(\sqrt{7} \times \sqrt{7})R19.1°$ overlayer for sulfide and bromide and the (8×8) overlayer for iodide). This behavior is exemplified in Figure 7a, which shows I vs t curves for different concentrations of bromide. Here, the current first decreases attaining a minimum, then increases up to a maximum, and finally tends asymptotically to zero. Obviously, the corresponding $Q(t)$ vs t curves in Figures 8−10 show two inflection points, in connection with the minimum and the maximum of the I vs t curves.

Firm evidence in favor of an initial diffusion-controlled adsorption is provided by plots of the charge density $Q(t)$ following the potential step against $t^{1/2}$ during the first 30−40 ms, before the onset of the PG process. These plots are linear, and their slopes are proportional to the bulk concentration c of the adsorbing anion, as shown in Figure 11 for bromide adsorption. The common intercept of the $Q(t)$ vs $t^{1/2}$ plots on the $t^{1/2} = 0$ axis measures the value, Q_0, of the charge density in the absence of the adsorbing anion at the same final potential. If adsorption is controlled by diffusion under limiting conditions (i.e., if the volume concentration of the adsorbing anion at the electrode surface is much smaller than the corresponding bulk value, c), then the integral form of the Cottrell equation states that the anion surface concentration $\Gamma(t)$ at time t is given by $2(Dt/\pi)^{1/2}c$. This implies that the slope, $[Q(t) - Q_0]/t^{1/2}$, of the $Q(t)$ vs $t^{1/2}$ plots equals $2(D/\pi)^{1/2}c[Q(t) - Q_0]/\Gamma(t)$. Under the reasonable assumption that the charge, $[Q(t) - Q_0]$, that flows

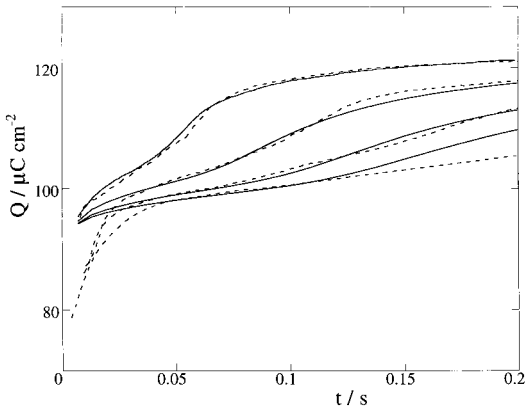

Figure 10. Charge vs time curves for bromide adsorption on Ag(111) obtained from 0.05 M KPF_6 solutions by stepping from −1.50 to −0.05 V. Proceeding from left to right, the KBr concentrations are 7.80×10^{-4}, 5.58×10^{-4}, 4.47×10^{-4}, and 3.35×10^{-4} M. The dashed curves are experimental plots; the solid ones were calculated as described in the text.

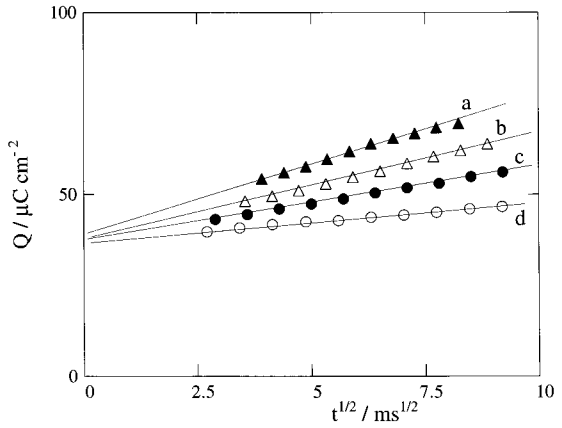

Figure 11. Plots of $Q(t)$ vs $t^{1/2}$ on Ag(111) from 0.05 M KPF_6 solutions containing 4.47×10^{-4} (a), 3.35×10^{-4} (b), 2.24×10^{-4} (c), and 1.12×10^{-4} M (d) KBr, as obtained by stepping from −1.50 to − 0.35 V.

as a consequence of progressive anion adsorption is proportional to $\Gamma(t)$, the slope of the $Q(t)$ vs $t^{1/2}$ plots is therefore expected to be proportional to c. The fact that such a proportionality is actually observed confirms a diffusion-controlled adsorption during the early stages of the charge transient.

Discussion

The behavior of the charge transients in Figures 3−5, obtained by stepping into the region of stability of the first overlayer, can be explained by the model in Appendix I, which accounts for diffusion of the adsorbing anions from the bulk solution toward the electrode, their RA, and the PG of the randomly adsorbed anions. The rate of the overall process is considered to be controlled by diffusion of the anions under limiting conditions and by PG, whereas RA is regarded as in quasi-equilibrium. It will be assumed that adsorbate−adsorbate interactions, which are mainly responsible for PG, and adsorbate−substrate interactions, which are responsible for chemisorption, affect anionic adsorption independently from each other. This assumption is justified when adsorbate−substrate interactions are not strictly directional. It is supported by the observation that STM images of halide ions adsorbed at single-crystal faces reveal the presence of structurally ordered islands at potentials slightly negative to those at which the surface becomes fully covered by an overlayer;[31] the same conclusions are suggested by the potential dependence of the intensity of the diffraction peaks in surface X-ray scattering.[58] Moreover, the preference of bromide adlayers on Au(100) for a structure close to hexagonal rather than the square c(2 × 2) structure, where the adatoms would reside in higher coordinated 4-fold hollow sites, suggests that the energy loss from the decrease in adsorbate−substrate interactions following the lack of occupation of 4-fold hollow sites only is more than compensated for by the energy gain from the increase in the strength of adsorbate−adsorbate interactions following the formation of the more compact hexagonal lattice.[47] This confirms the essential role played by adsorbate−adsorbate interactions, even in the case of partial charge transfer from the adsorbate to the substrate.

The model applies strictly to a "quasi-ideal" single-crystal face with only point defects (adatoms, vacancies, kinks) and monodimensional defects (monatomic steps), the remaining area consisting of regularly structured, uniform terraces. In this case, areas covered by randomly adsorbed anions cannot coexist at equilibrium with areas covered by clusters of a condensed phase, other than at the transition potential or, at most, over a very narrow potential range.[29] Consequently, in the potential region of stability of the condensed phase, randomly adsorbed anions will tend to organize themselves spontaneously into clusters, first subcritical and then supercritical in size. Polynucleation is regared as "heterogeneous". More precisely, adatoms, kinks, and monatomic steps are considered to act as nucleation centers. The initial number N_0 of nucleation centers per unit surface is therefore regarded as fixed and high enough to remain much greater than the time-dependent number $N(t)$ of nuclei practically up to full electrode coverage by the condensed phase, a familiar assumption in the treatment of PG.

The calculation of the $Q(t)$ vs t curves requires (i) the diffusion coefficient D of the adsorbing anion to account for its diffusion, (ii) its maximum surface concentration Γ_m to account for its RA, and (iii) a single parameter $K = k_R(\pi N_0 k_N)^{1/2}$, which embodies the rate constant k_N for nucleation as well as that, k_R, for the radial growth of clusters, to account for progressive PG. Values of the diffusion coefficient D were taken from the polarographic literature[59−62] and are summarized in Table 1. The Γ_m values for random adsorption were estimated by assuming that such an adsorption may take place, at least initially, at any possible site of the metal substrate (top sites, hollow sites, etc.). With this assumption, the maximum surface concentration that the randomly adsorbing anions would hypothetically attain from an entropic viewpoint, if there were no energetic limitations, corresponds to close packing. For the spherical anions under study, close packing is realized with a hexagonal lattice of lattice constant equal to the diameter d of the anion. From simple geometrical considerations it follows that $\Gamma_m = 2/(3^{1/2}d^2)$. Calculated values of Γ_m for the various anions are summarized in Table 1. Naturally, these hypothetical Γ_m values hold only at low surface coverages θ by the adsorbed anions, when RA takes place under diffusion limiting conditions; at higher coverages, short-range interactions prevent the actual attainment of these high Γ_m values. The model adopted herein also requires the specification of the number n of solute monomers composing a nucleus, i.e., the minimum cluster of monomers having a greater tendency to grow than to dissolve. Just as the analogous model adopted to interpret the 2D phase transitions of uracil on Ag(111),[10] the present model predicts calculated $Q(t)$ vs t curves that shift toward longer times as n is progressively increased up to 5−6 under otherwise identical conditions and then shift in the opposite direction with a further increase in n. Hence, the model points to an activationless incorporation of solute monomers into clusters consisting of

TABLE 1

	potential step	$D \times 10^5$ ($cm^2\ s^{-1}$)	$\Gamma_m \times 10^9$ (mol cm^{-2})	$\Delta\sigma_\theta$ ($\mu C\ cm^{-2}$)	$\Delta\sigma_S$ ($\mu C\ cm^{-2}$)	$\Delta\sigma_{SI}$ ($\mu C\ cm^{-2}$)	$k_R(\pi N_0 k_N)^{1/2}$ ($s^{-3/2}$)	$k_{R,I}(\pi k_{N,I})^{1/2}$ ($s^{-3/2}\ M^{-5/2}$)
S^{2-}	–							
	−1.35 V → −0.8 V	1.70	1.41	192	125	180	500	10
I^-	−1.5 V → −0.5 V	1.72	1.03	65	63	–	200	–
	−1.5 V → −0.2 V	1.72	1.03	25	(15)	40	500	10
Br^-	−1.5 V → −0.35 V	1.86	1.26	57	45	–	300	–
	−1.5 V → −0.05 V	1.86	1.26	17	(15)	35	500	10
Cl^-	−1.5 V → +0.15 V	1.82	1.48	120	55	–	6×10^3	–

more than about five monomeric units, namely, predicts a 5-meric nucleus. In what follows n will therefore be set equal to 5.

If we exclude the capacitive charge density that is required to charge the interphase following the potential step $E_i \rightarrow E$ and that flows within the first 1 or 2 ms from the instant of the potential step, the charge density $Q(t)$ flowing at a final potential E in the range of stability of the first overlayer is given by

$$Q(t) = \Delta\sigma_\theta\theta(t) + \Delta\sigma_S S(t),$$
$$\text{with } \Delta\sigma_\theta \equiv \sigma_\theta - \sigma_0,\ \Delta\sigma_S \equiv \sigma_S - \sigma_0$$

Here $\theta(t)$ and $S(t)$ are the time-dependent surface coverages by the randomly adsorbed anions and by the corresponding condensed phase; σ_0 is the charge density at E for an electrode in contact with a solution containing the supporting electrolyte in the absence of sulfide or halide ions; σ_θ and σ_S are the charge densities at E for an electrode fully covered by randomly adsorbed sulfide or halide ions and fully covered by the corresponding condensed phase, respectively. The quantity $\Delta\sigma_\theta$ was obtained from the slope, $[Q(t) - Q_0]/t^{1/2} = 2(D/\pi)^{1/2}c[Q(t) - Q_0]/\Gamma(t)$, of $Q(t)$ vs $t^{1/2}$ plots during the first stage of RA (see, e.g., Figure 11), upon multiplying $[Q(t) - Q_0]/\Gamma(t)$ by the calculated value of Γ_m. Values of $\Delta\sigma_\theta$ are reported in Table 1. The quantity $\Delta\sigma_S$ was estimated from $Q(E)$ vs E plots obtained by the chronocoulometric technique upon stepping from a progressively varied initial potential E to a fixed final potential E_f negative enough to exclude anionic adsorption.[63] Analogous $Q_0(E)$ vs E plots were obtained in the presence of the supporting electrolyte alone. The $Q(E)$ vs E plots run roughly parallel to the corresponding $Q_0(E)$ vs E plots over the potential range of stability of the ordered overlayer. The vertical distance between these two plots at the potential chosen for the charge transients in Figures 3−5 is therefore a measure of $\Delta\sigma_S$. Values of this quantity are summarized in Table 1.

The solid curves in Figures 3−5 are charge transients calculated on the basis of the model in Appendix I, using the parameters reported in Table 1; the corresponding experimental transients are represented by the dashed curves in the same figures. While the parameters $\Delta\sigma_\theta$ and $\Delta\sigma_S$ were obtained by independent means, as previously described, the kinetic parameter $K = k_R(\pi N_0 k_N)^{1/2}$ was chosen in such a way as to provide the best fit between calculated and experimental transients. The calculated transients do not include the c-independent double-layer charge flowing immediately after the potential step. Therefore, for comparison, the whole set of calculated transients, relative to the various concentrations c, was shifted as a whole along the vertical axis in order to achieve the best overlapping with the corresponding set of experimental transients. Agreement between experimental and calculated Q vs t curves can be regarded as satisfactory, when we consider that it was realized by using a single adjustable parameter, i.e., K, for the different anionic concentrations.

The model in Appendix I also accounts satisfactorily for the behavior of charge transients starting from an initial potential E_i at which the surface coverage θ by randomly adsorbed anions is not negligible. This is shown in Figure 6, where the dashed curves are experimental charge transients for iodide adsorption, obtained stepping from progressively less negative initial potentials E_i to a fixed final potential $E = -0.50$ V. The solid curves were calculated from the model for the same parameters as in Figure 3 (see Table 1), apart from the surface coverage θ, whose values were obtained from a thermodynamic analysis of chronocoulometric charge vs potential curves for iodide adsorption on Ag(111).[64] Agreement is once again good. The behavior in Figure 6 proves unequivocally that RA is the precursor of PG. Thus, the higher is the surface coverage by randomly adsorbed anions at the initial potential, the faster is the PG process at the final potential E and hence the shorter is the time at which the constant limiting charge is attained. If RA and PG proceeded in parallel on different surface areas, RA would not accelerate PG; rather, it would make a fraction of the electrode surface unavailable for PG.

2D Phase Transitions Leading to the Second Overlayer. The charge transients leading to the second, more compressed, overlayer are different in shape from those leading to the first overlayer. Thus, the former transients show two marked inflection points that are not present in the latter, as appears by comparing Figures 3−5 with Figures 8−10. The model in Appendix I, which implies a direct passage from RA to the second overlayer, is unable to account for this behavior. In fact, by following the same procedure as for the phase transition leading to the first overlayer, it was not possible to predict a minimum and a maximum in the calculated I vs t curves, nor two inflection points in the calculated Q vs t curves. The charge transients in Figures 8−10 can be tentatively explained by accounting for a disorder−order phase transition from the dilute phase to the first overlayer and for a further order−order phase transition from the first to the second overlayer. The resulting model is outlined in Appendix II. It assumes a diffusion-controlled RA of the anion from the bulk solution, which feeds the PG of the first overlayer; the PG of the second, more compressed, overlayer takes place inside the first overlayer and is fed both by the anions of the latter and by those coming from the solution adjacent to the surface area covered by the first overlayer. This model requires a further adjustable parameter $K_I = k_{R,I}(\pi k_{N,I})^{1/2}$, which embodies the rate constant $k_{N,I}$ of nucleation and that, $k_{R,I}$, of radial growth for the second overlayer. It also requires the number, n_I, of anions coming from the solution phase that are involved in the formation of a nucleus of the second condensed phase; n_I was set equal to 5, just as n. Unfortunately, there is no way to confirm this mechanism by a time-resolved STM imaging of the electrode surface, in view of the exceedingly high rate of formation of the more compressed overlayer.

The charge density $Q(t)$ flowing at a final potential E in the range of stability of the second overlayer is now given by

$$Q(t) = \Delta\sigma_\theta\theta(t) + \Delta\sigma_S S(t) + \Delta\sigma_{S,I} S_I(t),$$
$$\text{with } \Delta\sigma_\theta \equiv \sigma_\theta - \sigma_0,\ \Delta\sigma_S \equiv \sigma_S - \sigma_0,\ \Delta\sigma_{S,I} \equiv \sigma_{S,I} - \sigma_0$$

Here $S_I(t)$ is the surface coverage by the second overlayer, and $\sigma_{S,I}$ is the charge density at the final potential E for an electrode fully covered by the second overlayer. $\Delta\sigma_{S,I}$ was directly estimated from the vertical distance at the given potential E between the chronocoulometric $Q(E)$ vs E plots in the presence of the anion and those, $Q_0(E)$ vs E, obtained in the presence of the supporting electrolyte alone.[63] Values of $\Delta\sigma_{S,I}$ are summarized in Table 1. The solid curves in Figures 8−10 are calculated charge transients in best agreement with the corresponding experimental transients. In carrying out the fitting, the quantity $\Delta\sigma_S$ was treated as an adjustable parameter, since there is no way to estimate it by independent means. Its values are reported within parentheses in Table 1. Agreement between the experimental and calculated charge transients in Figures 8−10 is slightly less satisfactory than that in Figures 3−5, because of the higher number of simplifying assumptions involved in the model of Appendix II. Obviously, agreement between experimental and calculated current transients is worse than that between experimental and calculated charge transients. This is always the case when the predictions of a model yielding values of a function $f(x)$ of an independent variable x are compared with experimental plots of $df(x)/dx$ vs x, rather than with plots of the direct function $f(x)$. This is apparent by comparing the experimental curves of $I = dQ/dt$ vs t in Figures 2a and 7a with the corresponding curves in Figures 2b and 7b, calculated using the same parameters adopted for the Q vs t curves in Figures 3 and 10, respectively. The experimental I vs t curves in Figure 2a and 3a were obtained by numerical differentiation of the corresponding Q vs t curves, recorded directly by our computerized chronocoulometric system.

The fact that the experimental values of $\Delta\sigma_{S,I}$ for iodide and bromide ions are lower than the corresponding experimental values of $\Delta\sigma_S$, as measured over the potential range of stability of the first overlayer, may appear surprising. This is due to the fact that, over the more positive potential range of stability of the second overlayer, even the anions of the supporting electrolyte start to be appreciably adsorbed, causing an increase in the slope of the chronocoulometric Q_0 vs t plot for the supporting electrolyte alone. This is particularly true for 0.15 M NaOH, which had to be used as supporting electrolyte in order to shift the onset of hydrogen evolution to potentials negative to those at which iodide is completely desorbed. The supporting anion (OH^- for iodide and PF_6^- for bromide) is adsorbed during the first milliseconds from the instant of the potential step $E_i \rightarrow E$, because of its relatively high bulk concentration. Consequently, the charge $Q(t)$ that flows along the external circuit after the first milliseconds, to maintain the final potential E constant, consists not only of the positive contribution from the slow adsorption of halide ions but also of the smaller negative contribution from the concomitant desorption of the supporting anions displaced by the adsorbing halide ions.

Some Considerations on Anion−Anion Interaction Forces. Among the factors responsible for the increase in adsorptivity on Ag when passing from chloride to iodide, two are particularly relevant: (i) the corresponding decrease in halide−water interactions, testified by the decrease in single-ion hydration enthalpies;[65] (2) the corresponding decrease in electronegativity, which favors an increase in partial charge transfer to the silver substrate upon adsorption, as testified by a progressive increase in the electrosorption valency. Thus, chronocoulometric measurements of sulfide and halide adsorption on Ag(111) recently carried out in this laboratory[63] yield electrosorption valency values of −1.96 for sulfide, −0.86 for iodide, −0.77 for bromide, and −0.44 for chloride. These values point to an almost complete charge transfer for sulfide and iodide and a gradual decrease of the partial charge-transfer coefficient λ in passing to bromide and chloride. Standard quantum-mechanical CNDO calculations of λ for the chemisorption of hydrated halide ion complexes on a plane mercury atom cluster[66] also point to a progressive decrease of λ from iodide to chloride.

The relative extent of the different interactions coming into play during nucleation and growth is, therefore, expected to vary in passing from chloride to iodide and sulfide. Thus, ion−ion Coulombic repulsive forces are expected to decrease, in view of the progressively lower charge borne by the adsorbed ion. It should be noted, however, that Coulombic repulsive forces within the inner layer are notably screened by multiple imaging.[67] A decrease in the charge located in the adsorbed anion causes not only a decrease in the repulsive Coulombic interaction when two like adsorbed anions approach each other but also a decrease in the attractive cosphere overlap energy arising from the overlap of the Born polarization regions about the two ions.[68] The lower the charge on the adsorbed anion, the lower the Born polarization energy of its two-dimensional primary solvation sheath; hence, the decrease in the Born polarization of water in the overlap region, due to the opposing field vectors created by the two approaching anions, will also decrease. The two opposite contributions to the adion−adion pair potential are, therefore, expected to balance each other. Finally, once the primary hydration sheaths of the two approaching anions have overlapped, leaving practically a single adsorbed water molecule interposed between them, the squeezing out of the latter from the adsorbed state is favored by a further negative (i.e., attractive) "hydrophobic" contribution to the adion−adion pair potential: this is due to the increasing difficulty of the residual adsorbed water molecule to form H-bonds with neighboring adsorbed water molecules, resulting in its tendency to leave the adsorbed state so as to form H-bonds with bulk water molecules.[69] It is clearly impossible to quantify the various contributions to the overall interaction potential between adsorbed anions. At any rate, the very occurrence of 2D nucleation and growth indicates that the repulsive Coulombic interactions are more than compensated for by different types of attractive interactions, in addition to the usual van der Waals interaction forces.

Acknowledgment. The financial support of the Ministero dell'Universita'e della Ricerca Scientifica and of the Consiglio Nazionale delle Ricerche is gratefully acknowledged. Thanks are due to the Spanish DGICyT (Project PB94-0448) for financial support and to the Ministerio de Educación y Cultura, Spain, for a fellowship to A.F., during the tenure of which the present results were obtained. The authors are grateful to Mr. Andrea Pozzi and Mr. Francesco Gualchieri for technical assistance and to Mr. Ferdinando Capolupo for the preparation of the silver single-crystal electrodes.

Appendix I

The extended area S_x, namely, the hypothetical area per unit surface that would be covered by the growing clusters if their overlapping could be ignored, is expressed by the general relationship[70]

$$S_x = \int_0^t A(y,t)\, v_N(y)\, dy = g\int_0^t dy[\int_y^t v_R(z)\, dz]^2 v_N(y) \quad \text{(A1)}$$

with

$$v_R(t) \equiv \mathrm{d}R/\mathrm{d}t; \quad v_N(t) \equiv \mathrm{d}N/\mathrm{d}t$$

Here $A(y,t)$ is the area of a 2D cluster nucleated at time y and observed at time t, $v_N(t)$ is the rate of nucleation, $v_R(t)$ is the rate of radial growth of the cluster, and g is a geometrical factor that takes the value π in the simplest case of a circular cluster. Henceforth, we will constantly refer to circular clusters for simplicity. If we denote by n the number of monomers composing a nucleus, the elementary step that yields the nucleus consists of the incorporation of a monomer into an $(n-1)$-meric subcritical cluster; this is preceded by n elementary steps, which consist in the aggregation of a monomer to a nucleation center and subsequently in the incorporation of each monomeric unit into the immediately preceding subcritical cluster. If we assume that all these steps are in quasi-equilibrium, the nucleation rate will be proportional both to the number N_0 of nucleation centers and to the nth power θ^n of the electrode surface coverage by the randomly adsorbed anions, which constitute the monomeric units, according to a proportionality constant k_N:[10]

$$\mathrm{d}N/\mathrm{d}t = N_0 k_N \theta^n$$

The rate of growth of the area A of a circular cluster of radius R is given by the time derivative of πR^2. Moreover, it is proportional to the frequency of the impacts of the randomly adsorbed anions, of surface coverage θ, with the perimeter of the aggregate, $2\pi R$ in length, according to a proportionality constant k_R:

$$\mathrm{d}A/\mathrm{d}t = \mathrm{d}(\pi R^2)/\mathrm{d}t = 2\pi R\, \mathrm{d}R/\mathrm{d}t = k_R(2\pi R)\theta \Rightarrow \mathrm{d}R/\mathrm{d}t = k_R\theta$$

It follows that the rate of radial growth is proportional to θ. Upon substituting the above expressions for the rates of nucleation and of radial growth into the general expression of eq A1 for the extended area, carrying out some changes in the integration variables, and differentiating twice in order to convert the integral equation into a differential equation,[10] we get

$$\frac{\mathrm{d}^2 S_\mathrm{x}}{\mathrm{d}t^2} = 2K\sqrt{\frac{\mathrm{d}S_\mathrm{x}}{\mathrm{d}t}}\theta^{(n/2+1)} + \frac{n}{\theta}\frac{\mathrm{d}S_\mathrm{x}}{\mathrm{d}t}\frac{\mathrm{d}\theta}{\mathrm{d}t} \qquad \text{with } K \equiv k_R\sqrt{\pi N_0 k_N} \quad \text{(A2)}$$

where the parameter K embodies the rate constants for nucleation and for radial growth.

To solve the problem, it is now necessary to express θ as a function of time. In view of the high adsorptivity of the anions investigated, we may assume to a good approximation that their volume concentration at the electrode surface remains negligibly small with respect to that, c, in the bulk of the solution up to the attainment of full coverage by the condensed phase. Under these conditions the surface concentration Γ of the randomly adsorbed anions at time t is obtained by integrating over time the diffusional flux of the anions under limiting conditions, as expressed by the Cottrell equation, $(D/\pi t)^{1/2}c$, times the fraction of the electrode surface area, $(1-S)$, actually available for RA:

$$(1-S)\int_0^t \sqrt{\frac{D}{\pi t}}c\, \mathrm{d}t = 2(1-S)\sqrt{\frac{Dt}{\pi}}c = \Gamma = \Gamma_\mathrm{m}\theta \quad \text{(A3)}$$

In this equation Γ is set equal to the maximum surface concentration Γ_m times the surface coverage θ, by definition of surface coverage. Moreover, S is the fraction of the electrode surface area actually covered by the condensed phase; it is related to the corresponding extended area S_x by Avrami's equation:[71]

$$\mathrm{d}S/\mathrm{d}t = (1-S)\,\mathrm{d}S_\mathrm{x}/\mathrm{d}t \quad \text{(A4)}$$

Differentiating θ with respect to time in eq A3 yields

$$\frac{\mathrm{d}\theta}{\mathrm{d}t} = 2\sqrt{\frac{D}{\pi}}\frac{c}{\Gamma_\mathrm{m}}\left(\frac{1-S}{2t^{1/2}} - \frac{\mathrm{d}S}{\mathrm{d}t}t^{1/2}\right) \quad \text{(A5)}$$

The three differential equations (A2), (A4), and (A5) in the three unknown quantities θ, S, and $\mathrm{d}S_x/\mathrm{d}t$, with θ expressed by eq A3, can be readily solved numerically by the fourth-order Runge−Kutta method.

If the initial potential E_i is negative enough to exclude RA of the anion, the initial conditions are $\theta = 0$, $S = 0$, and $\mathrm{d}S_x/\mathrm{d}t = 0$. In practice, however, θ cannot be set exactly equal to zero at $t = 0$, because otherwise the right-hand side of eq A2 would tend to infinity. Analogously, $\mathrm{d}S_x/\mathrm{d}t$ cannot be set exactly equal to 0 at $t = 0$, when S is also equal to zero, because this would prevent PG from starting. Reliable solutions are obtained by ascribing to the initial values of θ and $\mathrm{d}S_x/\mathrm{d}t$ any nonzero positive value $\leq 1 \times 10^{-5}$; provided this requirement is satisfied, the numerical solution does not depend on the particular choice of the initial values. If at the initial potential E_i the surface coverage θ by randomly adsorbed anions assumes a nonzero value θ_in, then eqs A3 and A5 must be modified as follows:

$$\theta = \left(\theta_\mathrm{in} + 2\sqrt{\frac{Dt}{\pi}}\frac{c}{\Gamma_\mathrm{m}}\right)(1-S)$$

$$\frac{\mathrm{d}\theta}{\mathrm{d}t} = 2\sqrt{\frac{D}{\pi}}\frac{c}{\Gamma_\mathrm{m}}\left(\frac{1-S}{2t^{1/2}} - \frac{\mathrm{d}S}{\mathrm{d}t}t^{1/2}\right) - \frac{\mathrm{d}S}{\mathrm{d}t}\theta_\mathrm{in}$$

Appendix II

Let us examine the problem of a charge transient leading to the formation of the second overlayer via the intermediate formation of the first overlayer. Let us denote the actual surface coverage by the second condensed phase by S_I and the sum of the actual surface coverages by the two condensed phases by $S_\mathrm{t} \equiv S + S_\mathrm{I}$. The order−order 2D phase transition from the first to the second condensed phase does not affect S_t, whose growth in time is fed exclusively by the randomly adsorbed anions. Differently stated, on one hand the first condensed phase increases at the expense of the dilute phase, while on the other it decreases in favor of the second condensed phase. Therefore, the sum S_t increases exclusively at the expense of the dilute phase. Moreover, the fractional surface coverage available for RA is now $(1-S_\mathrm{t})$, rather than $(1-S)$. As a result, the three differential equations (A2), (A4), and (A5) of Appendix I can also be applied to the present case, provided we replace the actual and extended areas, S and S_x, of the first condensed phase by the actual and extended areas, S_t and $S_\mathrm{t,x}$, of the sum of the two different condensed phases:

$$\frac{\mathrm{d}^2 S_\mathrm{t,x}}{\mathrm{d}t^2} = 2K\sqrt{\frac{\mathrm{d}S_\mathrm{t,x}}{\mathrm{d}t}}\theta^{(n/2+1)} + \frac{n}{\theta}\frac{\mathrm{d}S_\mathrm{t,x}}{\mathrm{d}t}\frac{\mathrm{d}\theta}{\mathrm{d}t}$$

$$\frac{\mathrm{d}S_\mathrm{t}}{\mathrm{d}t} = (1-S_\mathrm{t})\frac{\mathrm{d}S_\mathrm{t,x}}{\mathrm{d}t}$$

$$\frac{d\theta}{dt} = 2\sqrt{\frac{D}{\pi}}\frac{c}{\Gamma_m}\left(\frac{1-S_t}{2t^{1/2}} - \frac{dS_t}{dt}t^{1/2}\right) \quad \text{(A6)}$$

The relationship between the actual surface area, S_I, covered by the second condensed phase and the corresponding extended area, $S_{I,x}$, is obtained by considerations analogous to those leading to Avrami's equation. Having assumed that the second condensed phase is formed exclusively at the expense of the first one, the hypothetical fractional surface area that would be covered by the growing clusters of the second condensed phase if their overlapping could be ignored is not the whole unit area, but rather the area S_t covered by both condensed phases. Conversely, the area actually available for the growth of the second condensed phase is that, $S = S_t - S_I$, covered by the first condensed phase. Following Avrami,[28,72] the rates of growth of S_I and of $S_{I,x}$ are proportional to the corresponding available areas, S and S_t, according to the same proportionality constant. Hence we have

$$dS_I/dt = kS; \quad dS_{I,x}/dt = kS_t$$

and also

$$dS_I/dt = (1 - S_I/S_t)\, dS_{I,x}/dt \quad \text{(A7)}$$

The dependence of $S_{I,x}$ upon the nucleation rate $\upsilon_{N,I}$ and upon the rate of radial growth, $\upsilon_{R,I}$, for the second condensed phase is expressed by the general relationship of eq A1. The rate of growth of the area $A_I = \pi R_I^2$ of a circular cluster of the second condensed phase is proportional to the frequency of the impacts of the anions of the first condensed phase with the cluster perimeter, $2\pi R_I$. Since the second condensed phase is assumed to grow inside the first one, a cluster of the second condensed phase is practically surrounded by the first condensed phase on all sides. Hence, in practice, dA_I/dt is just proportional to $2\pi R_I$ according to a proportionality constant that embodies the number density of the anions of the first condensed phase. We may therefore write

$$\frac{dA_I}{dt} = 2\pi R_I\frac{dR_I}{dt} = k_{R,I}(2\pi R_I) \rightarrow \upsilon_{R,I} \equiv \frac{dR_I}{dt} = k_{R,I} \quad \text{(A8)}$$

from which it follows that $\upsilon_{R,I}$ is independent of time. The nucleation rate, $\upsilon_{N,I}$, of the second condensed phase is proportional to the number density of the corresponding nucleation centers, which may be reasonably regarded as distributed uniformly on the surface area S of the first condensed phase; we will therefore set $\upsilon_{N,I}$ proportional to S. The formation of a nucleus of the second condensed phase inside the first one also requires the incorporation of a number n_I of anions coming from the solution phase, since the second phase is more compressed than the first one. We will assume that the concentration of the anions in the solution adjacent to the surface covered by the first condensed phase remains substantially proportional to the corresponding bulk value, c, despite the depletion of these anions following their initial RA. With these rough assumptions, $\upsilon_{N,I}$ is also proportional to the n_Ith power of c:

$$\upsilon_{N,I} = k_{N,I}Sc^{n_I} \quad \text{(A9)}$$

where $k_{N,I}$ is a proportionality constant. Substituting $\upsilon_{R,I}$ and $\upsilon_{N,I}$ from eqs A8 and A9 into the general eq A1, we get

$$S_{I,X} = \pi\int_0^t \upsilon_{N,I}\, dy[\int_y^t \upsilon_{R,I}\, dz]^2 = \pi k_{N,I}k_{R,I}^2\int_0^t Sc^{n_I}\, d(t-y)[\int_0^{t-y} d(z-y)]^2$$

$$= \pi k_{N,I}k_{R,I}^2\int_0^t Sc^{n_I}(t-y)^2\, d(t-y)$$

Differentiating $S_{I,x}$ with respect to time and substituting into eq A7, we obtain

$$dS_I/dt = (1 - S_I/S_t)\, dS_{I,x}/dt = (1 - S_I/S_t)\pi k_{R,I}^2 k_{N,I}c^{n_I}(S_t - S_I)t^2 \quad \text{(A10)}$$

The three differential equations of eq A6 and that of eq A10, in the four unknown quantities θ, S_t, $dS_{t,x}/dt$, and S_I, can be readily solved numerically by the fourth-order Runge−Kutta method.

References and Notes

(1) Stolberg, L.; Morin, S.; Richer, J.; Lipkowski, J. *J. Electroanal. Chem.* **1991**, *307*, 241.
(2) Hölzle, M. H.; Kolb, D. M. *Ber. Bunsen-Ges. Phys. Chem.* **1994**, *98*, 330.
(3) Scharfe, M.; Hamelin, A.; Buess-Herman, C. *Electrochim. Acta* **1995**, *40*, 61.
(4) Buess-Herman, C. *Prog. Surf. Sci.* **1994**, *46*, 335.
(5) Hölzle, M. H.; Wandlowski, Th.; Kolb, D. M. *Surf. Sci.* **1995**, *335*, 281.
(6) Wandlowski, Th.; Lampner, D.; Lindsday, S. M. *J. Electroanal. Chem.* **1996**, *404*, 215.
(7) Tao, N. J.; de Rose, J. A.; Lindsday, S. M. *J. Phys. Chem.* **1993**, *97*, 910.
(8) Wandlowski, Th. *J. Electroanal. Chem.* **1995**, *395*, 83.
(9) Hölzle, M. H.; Krznaric, D.; Kolb, D. M. *J. Electroanal. Chem.* **1995**, *386*, 235.
(10) Guidelli, R.; Foresti, M. L.; Innocenti, M. *J. Phys. Chem.* **1996**, *100*, 18491.
(11) Cavallini, M.; Aloisi, G.; Bracali, M.; Guidelli, R. *J. Electroanal. Chem.* **1998**, *444*, 75.
(12) Bort, H.; Jüttner, K.; Lorenz, W. J.; Schmidt, E. *J. Electroanal. Chem.* **1978**, *90*, 413.
(13) Blum, L.; Abruña, H. D.; Gordon, J. G.; Borges, G. L.; Samant, M. G.; Melroy, O. R. *J. Chem. Phys.* **1986**, *85*, 6732.
(14) Melroy, O. R.; Samant, M. G.; Borges, G. L.; Gordon, J. G.; Blum, L.; White, J. H.; McMillan, M.; Albarelli, M. J.; Abruña, H. D. *Langmuir* **1988**, *4*, 728.
(15) Samant, M. G.; Toney, M. F.; Borges, G. L.; Blum, L.; Melroy, O. R. *J. Phys. Chem.* **1988**, *92*, 220.
(16) Melroy, O. R.; Toney, M. F.; Borges, G. L.; Samant, M. G.; Kortright, J. B.; Ross, P. N.; Blum, L. *J. Electroanal. Chem.* **1989**, *258*, 403.
(17) Toney, M. F.; Gordon, J. G.; Borges, G. L.; Melroy, O. R.; Yee, D.; Sorensen, L. B. *Phys. Rev. B* **1994**, *49*, 7793.
(18) Magnussen, O.; Hotlos, J.; Nichols, R.; Kolb, D. M.; Behm, R. J. *Phys. Rev. Lett.* **1990**, *64*, 2929.
(19) Batina, N.; Will, T.; Kolb, D. M. *Faraday Discuss.* **1992**, *94*, 93.
(20) Manne, S.; Hansma, P. K.; Massie, J.; Elings, B. V.; Gewirth, A. A. *Science* **1991**, *251*, 183.
(21) Chen, C.; Wasburn, N.; Gewirth, A. A. *J. Phys. Chem.* **1993**, *97*, 9754.
(22) Ogaki, K.; Itaya, K. *Electrochim. Acta* **1995**, *40*, 1249.
(23) Carnal, D.; Oden, P. I.; Müller, U.; Schmidt, E.; Siegenthaler, H. *Electrochim. Acta* **1995**, *40*, 1223.
(24) Staikov, G.; Jüttner, K.; Lorenz, W. J.; Budevski, E. *Electrochim. Acta* **1994**, *39*, 1019.
(25) Lorenz, W. J.; Staikov, G. *Surf. Sci.* **1995**, *335*, 32.
(26) Hölzle, M. H.; Retter, U.; Kolb, D. M. *J. Electroanal. Chem.* **1994**, *371*, 101.
(27) Bhattacharjee, B.; Rangarajan, S. K. *J. Electroanal. Chem.* **1991**, *302*, 207.
(28) de Levie, R. In *Advances in Electrochemistry and Electrochemical Engineering;* Gerischer, H., Tobias, C. W., Eds.; Wiley: New York, 1985; Vol. 13, pp 1−67.
(29) Wandlowski, Th.; de Levie, R. *J. Electroanal. Chem.* **1993**, *352*, 279.
(30) Aloisi, G.; Funtikov, A. M.; Will, T. *J. Electroanal. Chem.* **1994**, *370*, 297.

(31) Foresti, M. L.; Aloisi, G.; Innocenti, M.; Kobayashi, H.; Guidelli, R. *Surf. Sci.* **1995**, *335*, 241.
(32) Tao, N. J.; Lindsay, S. M. *J. Phys. Chem.* **1992**, *96*, 5213.
(33) Haiss, W.; Sass, J. K.; Gao, X.; Weaver, M. J. *Surf. Sci.* **1992**, *274*, L593.
(34) Gao, X.; Weaver, M. *J. Am. Chem. Soc.* **1992**, *114*, 8544.
(35) Gao, X.; Weaver, M. J. *Phys. Rev. Lett.* **1994**, *73*, 846.
(36) Gao, X.; Edens, G. J.; Weaver, M. J. *J. Phys. Chem.* **1994**, *98*, 8074.
(37) Gao, X.; Edens, G. J.; Liu, F.-C.; Hamelin, A.; Weaver, M. J. *J. Phys. Chem.* **1994**, *98*, 8086.
(38) Ocko, B. M.; Watson, G. M.; Wang, J. *J. Phys. Chem.* **1994,** *98*, 897.
(39) Wang, J.; Watson, G. M.; Ocko, B. M. *Physica A* **1993**, *200*, 679.
(40) Yamada, T.; Batina, N.; Itaya, K. *Surf. Sci.* **1995**, *335*, 204.
(41) Magnussen, O. M.; Ocko, B. M.; Adzic, R. R.; Wang, J. *Phys. Rev. B* **1995**, *51*, 5510.
(42) Magnussen, O. M.; Ocko, B. M.; Wang, J. X.; Adzic, R. R. *J. Phys. Chem.* **1996**, *100*, 5500.
(43) Yau, S.-L.; Vitus, C. M.; Schardt, B. C. *J. Am. Chem. Soc.* **1990**, *112*, 3677.
(44) Vogel, R.; Baltruschat, H. *Ultramicroscopy* **1992**, *42*−*44*, 562.
(45) Vogel, R.; Baltruschat, H. *Surf. Sci.* **1991**, *259*, L739.
(46) Bittner, A. M.; Wintterlin, J.; Beran, B.; Ertl, G. *Surf. Sci.* **1995**, *335*, 291.
(47) Wandlowski, Th.; Wang, J. X.; Magnussen, O. M.; Ocko, B. M. *J. Phys. Chem.* **1996**, *100*, 10277.
(48) Dretschkow, Th.; Wandlowski, Th. *Ber. Bunsen-Ges. Phys. Chem.* **1997**, *101*, 749.
(49) Fawcett, W. R.; Mackey, M. D. *J. Chem. Soc., Faraday Trans. 1* **1973**, *69*, 634.
(50) Hills, G. S.; Reeves, R. H. *J. Electroanal. Chem.* **1971**, *31*, 269.
(51) Hamelin, A. In *Modern Aspects of Electrochemistry*; Conway, B. E., White, R. E., Bockris, J. O'M., Eds.; Plenum Press: New York, 1985; Vol. 16, p 1.
(52) Hamelin, A.; Stoicoviciu, L.; Doubova, L.; Trasatti, S. *J. Electroanal. Chem.* **1988**, *244*, 133.
(53) Herrmann, C. C.; Perrault, G. G.; Konrad, D.; Pilla, A. A. *Bull. Soc. Chim. Fr.* **1972**, *12*, 4468.
(54) Dickertmann, D.; Schultze, J. W.; Koppitz, F. D. *Electrochim. Acta* **1976**, *21*, 967.
(55) Aloisi, G. D.; Cavallini, M.; Innocenti, M.; Foresti, M. L.; Pezzatini, G.; Guidelli, R. *J. Phys. Chem. B* **1997**, *101*, 4774.
(56) Ocko, B. M.; Magnussen, O. M.; Wang, J. X.; Adzic, R. R.; Wandlowski, Th. *Physica B* **1996**, *221*, 238.
(57) Zei, M. S. *J. Electroanal. Chem.* **1991**, *308*, 295.
(58) Magnussen, O. M.; Ocko, B. M.; Wang, J. X.; Adzic, R. R. *J. Phys. Chem.* **1996**, *100*, 5500.
(59) Beran, P.; Bruckenstein, S. *Anal. Chem.* **1968**, *40*, 1044.
(60) Davis, D. G.; Everhart, M. E. *Anal. Chem.* **1964**, *36*, 38.
(61) Gallego, J. M.; Castellano, C. E.; Calandra, A. J.; Arvia, A. J. *J. Electroanal. Chem.* **1975**, *66*, 207.
(62) Peters, D. G.; Kinjo, A. *Anal. Chem.* **1969**, *41*, 1806.
(63) Foresti, M. L.; Innocenti, M.; Forni, F.; Guidelli, R. *Langmuir*, in press.
(64) Foresti, M. L.; Innocenti, M.; Kobayashi, H.; Guidelli, R., unpublished results.
(65) Conway, B. E. *Electrochemical Data*; Elsevier: Amsterdam, 1952; p 132.
(66) Kuznetsov, An.; Reinhold, J.; Lorenz, W. *Electrochim. Acta* **1984**, *29*, 801.
(67) Pezzatini, G.; Innocenti, M.; Foresti, M. L.; Guidelli, R. *J. Phys. Chem. B* **1997**, *101*, 2306.
(68) Conway, B. E. *Elektrokhimiya* **1977**, *13*, 822; *J. Electroanal. Chem.* **1981**, *123*, 81.
(69) Guidelli, R.; Aloisi, G. *J. Electroanal. Chem.* **1994**, *373*, 107.
(70) Bosco, E.; Rangarajan, S. K. *J. Chem. Soc., Faraday Trans. 1* **1981**, *77*, 483.
(71) Avrami, M. *J. Chem. Phys.* **1939**, *7*, 1103.
(72) Avrami, M. *J. Phys. Chem.* **1940**, *8*, 212.